IOP Publishing
ICNFP 2021

Focus on New Frontiers in Physics - Selected Papers from

Physica Scripta **XX** (XXXX) XXXXXX https://doi.org/XXXX/XXXX

ATLAS searches for Higgs boson decays to BSM dark-Z bosons in four-lepton final states

Theodota Lagouri[1]

On behalf of the ATLAS Collaboration

[1] UTA, Instituto de Alta Investigación, Universidad de Tarapacá, Arica, Chile

E-mail: theodota.lagouri@cern.ch

Received xxxxxx
Accepted for publication xxxxxx
Published xxxxxx

Abstract

ATLAS searches for a BSM light boson using events where a Higgs boson with mass 125 GeV decays to four leptons are reported. This decay is presumed to occur via an intermediate state which contains one or two on-shell, promptly decaying bosons: $H \rightarrow ZX/XX \rightarrow 4l$, where X is a new dark vector boson Z_d (or a pseudo-scalar a), with an invariant mass between 1 and 60 GeV. These exotic Higgs decays searches use 139 fb^{-1} of p-p collision (Run-2) data at $\sqrt{s}$=13 TeV collected with the ATLAS detector at the LHC. The results are found to be consistent with SM background predictions and both fiducial model-independent limits as well as limits with interpretations in specific benchmark theory models are set.

Keywords: BSM, Higgs, dark-*Z*

1. Introduction

Despite the discovery of the Higgs boson at the Large Hadron Collider (LHC) in 2012 [1, 2], there is reason to suspect that the Standard Model's (SM) explanation of the Higgs sector is still incomplete. Astrophysical observations implying the existence of dark matter motivate extensions to the Higgs sector of the SM, particularly those that propose the existence of a 'dark' (i.e., hidden) sector with its own hidden-sector particles, in addition to the well-known issues of naturalness and baryon asymmetry.

Non-standard ('exotic') Higgs boson decays are an appealing technique to look for new physics in the Higgs sector. Existing precision measurements of the properties of the Higgs boson still allow non-standard decays to have a branching ratio of up to around 10% (provided that the Higgs boson's couplings to the W and Z bosons are not greater than their SM values) [3–5]. Furthermore, because the Higgs boson's decay width is predicted to be relatively narrow by the SM, even a minor coupling to a new light state could result in a large branching ratio to that state. New hidden-sector particles may also preferentially couple to the Higgs boson, making it a 'portal' into this new physics [6–9]. Many proposed extensions to the SM predict exotic Higgs boson decays, including models with a first-order electroweak phase transition [10, 11], neutral naturalness [12–14], and a hidden sector [15–25], as well as several dark matter models [26–31], including some posited to explain observed astrophysical positron excesses [32–34]. The Next-to-Minimal Supersymmetric Standard Model (NMSSM) [35–40] also predicts them.

1.1 ATLAS Searches for Dark-Z Bosons

The data used in this research come from 139 fb^{-1} of $\sqrt{s}$=13 TeV proton-proton (pp) collision data obtained with the ATLAS detector between 2015 and 2018 [41]. Nearly the full solid angle surrounding the collision point is covered by the ATLAS detector [42] at the LHC. It includes a muon spectrometer with three large superconducting air-core toroidal magnets, electromagnetic and hadron calorimeters and an inner tracking detector encircled by a thin superconducting solenoid. The expected contributions from

both the signal processes and most background processes are determined using Monte Carlo (MC) simulation [41].

This study describes three separate searches for the SM Higgs boson H decaying via a new boson into a final state containing four charged leptons ($l \equiv e, \mu$). The new boson might be a dark-sector vector boson or a scalar boson, indicated by X, according to the models that motivated these investigations.

The following are the three searches that have been considered:

- High-mass (HM): $H \rightarrow XX \rightarrow 4l$ (15 GeV< m_X< 60 GeV).
- Low-mass (LM): $H \rightarrow XX \rightarrow 4\mu$ (1 GeV <m_X <15 GeV).
- Single Z boson (ZX): $H \rightarrow ZX \rightarrow 4l$ (15GeV<m_X<55 GeV).

Finding two same-flavour opposite-sign lepton pairs with an overall invariant mass consistent with the decay of a SM Higgs boson is the goal of all three analyses covered in this study. Because the selection efficiency for isolated muons is substantially higher than that for isolated electrons in this mass range, the LM analysis only employs the 4μ final state. These searches are sensitive to any intermediate bosons that are narrow, on-shell, and decay promptly within the mass ranges investigated. Model-independent fiducial cross-section limits, as well as limits depending on the specific models mentioned in Section 4, are presented in this study.

This research builds on ATLAS prior searches, which included 20 fb^{-1} of data collected at $\sqrt{s}$ = 8 TeV [43] and 36 fb^{-1} of data collected at $\sqrt{s}$ = 13 TeV [44]. The signal region selection of the HM analysis has been re-optimized, in addition to a larger data sample and enhanced lepton detection. ATLAS [45–49] and CMS [50–52] have conducted comparable searches, including searches for pairs of light bosons decaying into muons, τ-leptons, photons, and/or jets, using both $\sqrt{s}$ = 8 TeV and 13 TeV data. Refs. [53, 54] report on additional searches for an SM Higgs boson decaying into undiscovered particles.

1.1.1 Benchmark Models

Two well-motivated benchmark models for exotic decays to light BSM bosons are summarized below, and they are utilized to interpret the results in this paper. The SM is extended with a dark-sector $U(1)$ group, abbreviated $U(1)_d$, in the first BSM benchmark model, resulting in the development of a BSM vector boson, Z_d. Two Higgs doublets and an extra singlet scalar field (2HDM+S) are present in the second BSM benchmark model. A BSM pseudoscalar boson, a, appears as a result of this. In the decays $H \rightarrow ZX \rightarrow 4l$ and $H \rightarrow XX \rightarrow 4l$, the Z_d boson and the a pseudoscalar might both represent the intermediate state, with the first benchmark model chosen for a higher mass range and the second for a lower mass range.

With an additional $U(1)_d$ dark gauge symmetry [19–24], a dark sector is introduced, which is related to the SM via kinetic mixing ε with the hypercharge gauge field [55–57]. The Z_d vector boson is the symmetry's gauge boson. The gauge coupling determines the branching ratios of the Z_d, which are independent of the kinetic mixing strength ε. Because of this coupling, a large percentage of decays (15%) result in pairs of electrons or muons. For Z_d masses of 1 to 60 GeV, the decay would be prompt (compared to the ATLAS detector's vertex resolution) for $\varepsilon > 10^{-5}$ [19]. The misplaced decays produce a distinctive signal for smaller values of ε. The decay products would be extremely collimated for Z_d masses below a few GeV and tiny values of ε and would require a specific study. ATLAS and CMS have searched for these long-lifetime signatures in collisions at energies of both 8 TeV [58-61] and 13 TeV [62-66].

Another theory is that the Z boson and Z_d mass combine, allowing the Z_d to decay to SM particles more easily. The strength of the mixing in this process is governed by the mass mixing parameter δ [19, 43]. There could be mixing between the SM Higgs boson and the dark Higgs boson, s, if the $U(1)_d$ symmetry is broken by the introduction of a dark Higgs boson [19–24]. The Higgs portal coupling, κ, governs the strength of the Higgs coupling to dark vector bosons in this scenario. The observed Higgs boson is the lightest in an extended Higgs sector, and it could decay into dark-sector particles.

The decay $H \rightarrow ZZ_d$ probes the parameter space of ε and m_{Zd} for the processes described in this study, and is independent of the occurrence of mixing between the SM Higgs boson and the dark-sector Higgs boson, κ. On an event-by-event basis, however, this BSM signal is indistinguishable from SM $H \rightarrow ZZ$, and hence must originate as a resonance in the dilepton mass above this background process. The SM background to the $H \rightarrow Z_dZ_d$ process, on the other hand, is easier to distinguish from the signal. This property makes the latter channel susceptible to significantly lower kinetic mixing values, with the sole need being that the kinetic mixing be large enough for the Z_d to decay quickly. However, because mixing between the SM Higgs boson and the dark-sector Higgs boson is required for this process, it explores the parameter space of κ and m_{Zd}.

Figures 1(a) and 1(b) depict the processes investigated in this study, which include a SM Higgs boson decaying into Z_d bosons and are included in the Hidden Abelian Higgs Model (HAHM) [19]. The search for $H \rightarrow aa \rightarrow 4\mu$ is pertinent to models with two Higgs doublets and an extra scalar field (2HDM+S) [20, 67]. Two-Higgs-doublet models (2HDMs) have two neutral scalars $H_{1,2}$, two charged scalars $H^{\pm}$, and one neutral pseudoscalar A in general. The measured Higgs boson H is identified as the lighter of the neutral scalars H_1, while the other states are limited to be heavy by current data [68, 69]. A scalar, s, and a pseudoscalar, a, are created by adding a complex scalar singlet that mixes weakly with $H_{1,2}$. If these are less than $m_H/2$, $H \rightarrow aa$ and $H \rightarrow ss$ decays are permitted (Figure 1(c)). This work investigates the process $H \rightarrow aa \rightarrow 4\mu$, although the same constraints that apply to $H \rightarrow aa \rightarrow 4\mu$, also apply to $H \rightarrow ss \rightarrow 4\mu$.

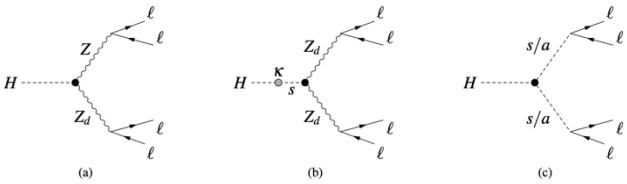

Figure 1: *Exotic Higgs boson decays into four leptons via (a) the hypercharge portal (to which the ZX analysis is sensitive) and (b) the Higgs portal, where s is a dark Higgs boson [19] (to which the HM and LM analyses are sensitive). Through kinetic mixing with the hypercharge field, the Z_d gauge boson decays into SM particles (with branching ratios that are nearly independent of ε). While the HZZ_d vertex factor is proportional to ε, the HZ_dZ_d vertex factor is proportional to κ. In models with an extended Higgs sector, (c) depicts the decay of a Higgs boson into dark Higgs scalars s or pseudoscalars a that couple to SM particles by mixing with the SM Higgs field [41].*

The presence of the dark sector could be deduced from Higgs boson decays through novel intermediate states or deviations from the SM-predicted rates of Drell-Yan (DY) events. Because the LHC experiments are the only ones sensitive to the generation of Higgs bosons, the search for the presence of a Higgs portal proposed here is possible. The $H\rightarrow Z_dZ_d \rightarrow 4l$ search is used to probe constraints on the Higgs mixing parameter κ, whereas the $H\rightarrow ZZ_d \rightarrow 4l$ search is used to get constraints on the kinetic mixing parameter ε, and the mass-mixing parameter δ.

2. Analysis Overview

All three studies in this study look for mass resonances in final states containing a quadruplet of two same-flavour opposite-sign (SFOS) lepton pairs: (e^+e^- + e^+e^-), (e^+e^- + $\mu^+\mu^-$), or ($\mu^+\mu^-$ + $\mu^+\mu^-$). m_{12} and m_{34} are the invariant masses of the two pairings, with m_{12} being the one closest in mass to the Z boson and $|\, m_{12} - m_Z \,| < |\, m_{34} - m_Z \,|$.

A Higgs boson decays into a pair of new bosons X, or into a new boson X and a Z boson, which decay into pairs of leptons in all of the analyses. Assuming that the X bosons are on-shell, the technique is to look for resonances in the relevant dilepton mass distributions. Each analysis creates a signal region (SR) by making a set of choices on measured parameters that enhance the signal's sensitivity.

The preselection is the same in all three studies, but the subsequent stages of picking candidate final-state leptons, forming them into quadruplets, selecting one of those quadruplets, and applying additional conditions to the picked quadruplet differ. The event selections for the various analyses are shown in Table 1.

Table 1: *For the ZX, HM, and LM analyses, a summary of event selection requirements. The $m_{J/\psi}$ = 3.096 GeV, $m_{\psi(2S)}$ = 3.686 GeV, $m_{\Upsilon(1S)}$ = 9.461 GeV, and $m_{\Upsilon(3S)}$ = 10.355 GeV are the quarkonia masses [70],[41].*

		Single Z (ZX) analysis $H \rightarrow ZX \rightarrow 4\ell$ ($\ell = e, \mu$)	High-mass (HM) analysis $H \rightarrow XX \rightarrow 4\ell$ ($\ell = e, \mu$)	Low-mass (LM) analysis $H \rightarrow XX \rightarrow 4\mu$
Mass range		15 GeV < m_X < 55 GeV	15 GeV < m_X < 60 GeV	1 GeV < m_X < 15 GeV
Baseline electrons		p_T > 7 GeV and $\|\eta\|$ < 2.47 Loose identification with an IBL hit $\|z_0 \sin\theta\|$ < 0.5 mm		—
Baseline muons		p_T > 5 GeV (15 GeV if calo-tagged) and $\|\eta\|$ < 2.7 Loose identification $\|z_0 \sin\theta\|$ < 0.5 mm and d_0 < 1 mm (except for standalone muons)		
Quadruplet selection		Require at least one quadruplet consisting of two pairs of same-flavour opposite-sign leptons Three leading-p_T leptons satisfying p_T > 20 GeV, 15 GeV, 10 GeV Number of calorimeter-tagged muons plus number of standalone muons not greater than 1 At least one lepton in the quadruplet responsible for firing at least one trigger For di-lepton triggers, all leptons of the trigger must match leptons in the quadruplet Define pairs m_{12} and m_{34} such that $\|m_{12} - m_Z\| < \|m_{34} - m_Z\|$		
		50 GeV < m_{12} < 106 GeV 12 GeV < m_{34} < 115 GeV $m_{14,32}$ > 5 GeV ($4e/4\mu$)	—	
		$\Delta R(\ell, \ell')$ > 0.10 (0.20) for same-flavour (different-flavour) leptons in the quadruplet		—
Quadruplet ranking		In order 4μ, $2e2\mu$, $2\mu2e$, $4e$ Smallest $\|m_Z - m_{12}\|$ Smallest $\|m_Z - m_{34}\|$	Select quadruplet with smallest $\Delta m_{\ell\ell} = \|m_{12} - m_{34}\|$	
Event selection	Isolation & impact parameter	Track and calorimeter isolation Excluding tracks/clusters from other leptons in the quadruplet d_0/σ_{d_0} < 5 for electrons and d_0/σ_{d_0} < 3 for muons		
	$m_{4\ell}$	115 GeV < $m_{4\ell}$ < 130 GeV		120 GeV < $m_{4\ell}$ < 130 GeV
	Z-veto	—	10 GeV < $m_{12,34}$ < 64 GeV For $4e$ and 4μ channels: 5 GeV < $m_{14,23}$ < 75 GeV	—
	Heavy-flavour veto	—	Reject event if $m_{12,34,14,23}$ in: ($m_{J/\Psi}$ − 0.25 GeV) to ($m_{\Psi(2S)}$ + 0.30 GeV), or ($m_{\Upsilon(1S)}$ − 0.70 GeV) to ($m_{\Upsilon(3S)}$ + 0.75 GeV)	
	Signal region	—	$m_{34}/m_{12} > 0.85 - 0.1125\, f(m_{12})$	1.2 GeV < $m_{12,34}$ < 20 GeV m_{34}/m_{12} > 0.85 Reject event if $m_{12,34}$ in: 2 GeV to 4.4 GeV, or 8 GeV to 12 GeV

2.1 Analysis - High Mass (HM)

The high-mass analysis selects events that are consistent with $H \rightarrow XX \rightarrow 4l$ decays based on a set of kinematic constraints. The four-lepton system's invariant mass must be consistent with the SM Higgs boson: 115 < GeV m_{4l} < 130 GeV. Furthermore, the lepton pairs must be incompatible with the decays of Z bosons (Z-veto): 10 GeV < $m_{12,34}$ < 64 GeV. It is possible that the leptons from a single X or Z decay are not linked together in the $4e$ and 4μ channels, but that a lepton from one Z/X decay may be paired with a lepton from the other Z/X decay. In order to suppress ZZ^* background events in which the leptons are mispaired, there are further requirements on the alternative lepton pairings, 5 GeV < $m_{14,23}$ < 75 GeV. With constraints on the lepton pair masses, events with pairs consistent with J/ψ or Y decay are likewise rejected (see Table 1).

The final criteria ensures that m_{12} and m_{34} are consistent: $m_{34}/m_{12} > 0.85 - 0.1125\, f(m_{12})$, where $f(m_{12})$ is ~1 at m_X =15 GeV and 0 for m_X >50 GeV (defined in [41]). As illustrated in Figure 2(b), this defines a wedge-shaped region in the m_{12}– m_{34} plane when combined with the relation $|\, m_{12} - m_Z \,| < |\, m_{34} - m_Z \,|$.

Simulation [41] is used to estimate the backgrounds with four prompt leptons, which are then validated using data from background-dominated control samples. $H \rightarrow ZZ^* \rightarrow 4l$ (about 72% of the total background) and $ZZ^* \rightarrow 4l$ (about 24% of the total background) are the most common

backgrounds. The $tt\bar{Z} \rightarrow 4l$ and processes with three-gauge bosons are examples of similar processes. These are discovered to be insignificant.

Processes containing leptons originating from the decay of heavy-flavour jets, or jets misidentified as leptons, are among the reducible backgrounds. Data is used to estimate the background from the Z + jets procedure. This gives a background estimate for the Z + jets process in the signal region that is compatible with zero. Simulation is used to estimate other reducible backgrounds. The most significant contribution comes from $t\bar{t}$, which accounts for around 3% of the entire background. Other similar backgrounds are shown to be insignificant, such as di-boson synthesis and heavy flavour processes. Four dedicated background-enriched validation zones, chosen so that they do not overlap with the HM signal region, are used to verify the background estimations.

2.2 Analysis - Low Mass (LM)

The LM analysis was created to be sensitive to the mass range of 1 GeV < m_X < 15 GeV. The angular distance between the two leptons in the $X \rightarrow ll$ decay can become very narrow for these low masses (ΔR (l, l) < 0.1 for m_X = 1 GeV). Because the efficiency of selecting electrons is much lower than that of muons, this analysis only considers the 4μ final state. Except for a few kinematic criteria, the event selection is fairly like that of the HM analysis (Section 2.1). The Z-veto condition is no longer applicable, and the ΔR requirements between final-state leptons have been removed. The two lepton pair masses m_{12} and m_{34} must not be in the ranges 2–4.4 GeV or 8–12 GeV, in addition to the HM heavy-flavour veto. Because muons have lower radiative losses than electrons, the m_{4l} requirement is reduced to 120 GeV < m_{4l} < 130 GeV, and both lepton pairs must satisfy 1.2 GeV < $m_{12,34}$ < 20 GeV. In addition, the signal region's ultimate requirement is reduced to m_{34} / m_{12} > 0.85.

The four prompt lepton backgrounds are estimated directly from MC simulations [41]. The $H \rightarrow ZZ^* \rightarrow 4\mu$ and $ZZ^* \rightarrow 4\mu$ processes account for almost two-thirds of the total background estimate. Higher-order electroweak processes, such as triboson production and vector-boson scattering, are discovered to be insignificant. Non-prompt leptons are present in the remaining backgrounds, mostly from decays of heavy-flavour hadrons in events involving multiple b-quarks, such as $b\bar{b}$. Double semi-leptonic decays, in which a b-hadron decays into a muon and a c-hadron, which then decays into another muon and light hadrons, account for a large portion of this contribution. The heavy-flavour vetoes on dilepton masses necessary as part of the LM event selection suppress the resonances created in the b-hadron decay chain (i.e., ω, ρ, ϕ, J/ψ). There is also a minor contribution from $b\bar{b}b\bar{b}$, where each muon comes from its own b-quark. B-jet tagging isn't beneficial for minimizing these backgrounds because the muons chosen are all isolated. A data-driven strategy is used to estimate the backgrounds of these processes. On the heavy-flavour background yield, the overall systematic uncertainty is calculated to be 50%.

2.3 Analysis - ZX

The ZX analysis varies from the HM and LM analyses in that it includes the selection of a Z boson as well as a new X boson. It is, nevertheless, very comparable to the ATLAS SM $H \rightarrow ZZ^* \rightarrow 4l$ analysis selection [71]. In addition to the common conditions specified in Section 2, each quadruplet must meet the following requirements: 50 GeV < m_{12} < 106 GeV, 12 GeV < m_{34} <115 GeV, and $m_{14,\,23}$ > 5 GeV for the $4e$ and 4μ channels. The latter criterion is sufficient to exclude mismatched J/ψ events. After all selections, the background from Y decays was found to be minimal. If more than one such quadruplet exists, the quadruplets are ranked using the following criteria, which are applied in order:

- Sort the two lepton pairs by their flavours in order of expected efficiency. Muons have a higher reconstruction efficiency than electrons, hence $4\mu > 2e2\mu > 2\mu2e > 4e$.
- Pick the quadruplet with the smallest $|m_Z - m_{12}|$.
- Pick the quadruplet with the smallest $|m_Z - m_{34}|$.

This rule applies to all quadruplets, even those of the same flavour. The alternate pairing is handled as a separate quadruplet for this study and is included in the quadruplet ranking and selection. The additional HM analysis conditions (Z boson/heavy-flavour veto and signal region restrictions) are not implemented here.

$H \rightarrow ZZ^* \rightarrow 4l$ (about 65% of the total) and non-resonant $ZZ^* \rightarrow 4l$ are the most common backgrounds in this study (about 33% of the total). The triboson processes ZZZ, WZZ, and WWZ provide additional prompt backgrounds. These are calculated via simulation [41], but the $ZZ^* \rightarrow 4l$ background estimate is validated with background-enriched validation samples. Other, reducible backgrounds, such as Z + jets, $t\bar{t}$, and WZ processes, comprise only a few percent of the background and contain either extra non-isolated leptons from heavy-flavour decay or objects misinterpreted as leptons. The ATLAS SM $H \rightarrow ZZ^* \rightarrow 4l$ analysis employed the same data-driven technique to estimate the total yield of these backgrounds [71, 72]. Finally, simulation is used to determine the shape of the m_{34} distribution for the reducible background. Due to variations in the lepton isolation requirements between this study and the ATLAS SM $H \rightarrow ZZ^* \rightarrow 4l$ analysis, the reducible background estimate has a 10% systematic uncertainty.

3. Analysis Results

All of the analyses considered here share a number of systematic uncertainties. Among the most prominent are: 1) Luminosity and pile-up: The integrated luminosity has a 1.7% uncertainty [73, 74]. Approximately 1% of the uncertainty is attributable to pile-up. 2) Uncertainties about leptons: The efficiency with which events pass selection is determined by the leptons' reconstruction and identification efficiencies, as well as their momentum scale determination [75, 76]. Because the final state has four leptons, minor single-lepton uncertainties can lead to greater final yield uncertainties of up to 15%, which are dominated by the uncertainty in electron reconstruction and identification efficiency. 3) Uncertainties in theory: Variations in the parton distribution functions, factorization, renormalization, and QCD scales, as well as the modelling of hadronization and the underlying event, are used to assess uncertainties in the simulation of signal and background processes. The total uncertainty in signal acceptance is roughly 3%, while the background yield uncertainty is 3–9% for the $H \rightarrow ZZ^* \rightarrow 4l$ process [77] and about 5% for $ZZ^* \rightarrow 4l$ [78-83].

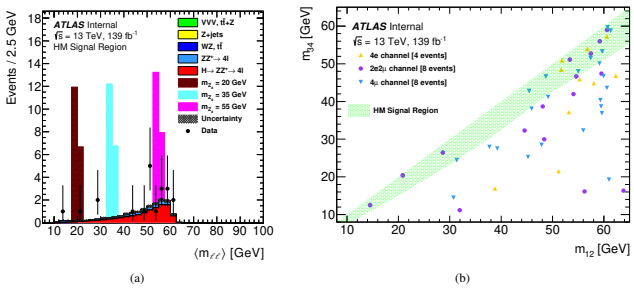

Figure 2: *For events selected in the HM $H \rightarrow XX \rightarrow 4l$ (15 GeV < m_X < 60 GeV) study, distribution of (a) $\langle m_{ll} \rangle$ and (b) m_{34} vs. m_{12}. The (pre-fit) background expectations are also represented in the $\langle m_{ll} \rangle$ distribution (a); the hatching band encompasses the statistical and systematic uncertainty. For certain masses, the signal's expectations are also shown. The predicted yields are normalized using $\sigma(pp \rightarrow H \rightarrow Z_d Z_d \rightarrow 4l) = {}^{1/10}\,\sigma_{SM}(pp \rightarrow H \rightarrow ZZ^* \rightarrow 4l)$ = 0.60 fb (ggF process only), and the signal histograms are stacked on top of the background histograms. The uncertainties of the plotted data are asymmetric and are calculated using Eqs. (40.76) from the 2020 Review of Particle Properties [70]. Each marker corresponds to an event that passes the Higgs boson window requirement and Z boson veto in the m_{34} vs. m_{12} distribution (b). The events of the signal region are represented by the markers (differentiated by channel) that fall within the green shaded area, [41].*

3.1 High Mass (HM): H⟶XX⟶4l (15 GeV< m_X<60 GeV)

The high-mass analysis looks for SM Higgs boson decays to a pair of new bosons X, where X can be Z_d, a, or s, which decay to pairs of electrons or muons. Finding two same-flavour opposite-sign pairs of leptons of equal invariant mass that are consistent with the decay of a SM Higgs boson but inconsistent with the decay of Z bosons is required for event selection.

Table 2 summarizes the final yields and uncertainties in the signal region indicated in Table 1, while Fig. 2 (a) shows the resulting $\langle m_{ll} \rangle$ distribution for this search. There are a total of 20 events, with an expected background of 15.6 ± 1.3 events. The test statistic is the profile-likelihood ratio. Around m_{Zd} = 28 GeV, the highest deviation from SM expectations occurs, corresponding to an event with $\langle m_{ll} \rangle \approx$ 28 GeV and a local significance of 2. 5σ. Figure 2(b) depicts the distribution of m_{34} versus m_{12} for the selected events.

Table 2: *SM background processes expected event yields and data for the HM $H \rightarrow XX \rightarrow 4l$ (15 GeV < m_X < 60 GeV) selection. Three of the 20 observed events are beyond the range 15 GeV < $\langle m_{ll} \rangle$ < 60 GeV and hence are not considered when setting limits. The systematic uncertainty in background estimates is highly correlated across different background sources, [41].*

Process	Yield (±stat. ± syst.)
$H \rightarrow ZZ^* \rightarrow 4\ell$	$11.1 \pm 0.1 \pm 1.0$
$ZZ^* \rightarrow 4\ell$	$3.38 \pm 0.05 \pm 0.25$
$t\bar{t}$	$0.47 \pm 0.13 \pm 0.09$
Z + jets	$0.43 \pm 0.39^{+0.17}_{-0.01}$
$Z + t\bar{t} \rightarrow 4\ell$	$0.09 \pm 0.02 \pm 0.02$
WZ	$0.05 \pm 0.03^{+0.05}_{-0.00}$
VVV/VBS	Negligible
Heavy flavour	Negligible
Total	$15.6 \pm 0.4 \pm 1.2$
Data	20

3.2 LM analysis: H⟶XX⟶4μ (1 GeV< m_X < 15 GeV)

The LM analysis extends the HM analysis to the 1 GeV < m_X <15 GeV area, where $X = Z_d$, a, or s. For this analysis, only the 4μ final state is considered. With certain fine-tunes for the different kinematic regions, the event selection is comparable to that of the HM analysis.

Figure 3 (a) depicts the $\langle m_{ll} \rangle$ distribution in the LM signal region (a). Figure 3 (b) describes the m_{12} vs. m_{34} distribution, whereas Table 3 summarizes the final yields and uncertainties. With a total background prediction of 0.89 ± 0.15 events, no events are detected.

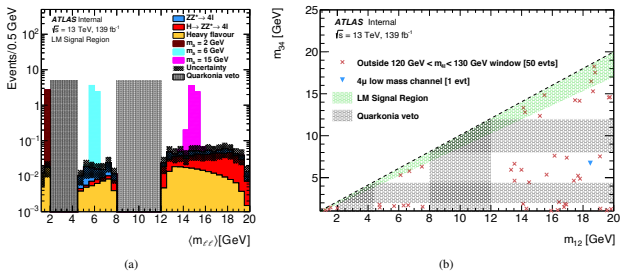

Figure 3: *For events selected in the LM H⟶ XX⟶ 4μ (1 GeV < m_X < 15 GeV) study, distribution of (a) ⟨m_{ll}⟩ and (b) m_{34} vs. m_{12}. There are no data events that pass the criteria. For certain masses, the expectation for H⟶ aa⟶4μ signal is also shown. The predicted yields are normalized using σ (pp → H → aa → 4μ) = $^{1/10}$ σ_{SM} (pp⟶ H → ZZ* → 4μ) = 0.15 fb (ggF process only), and the signal histograms are layered on top of the (pre-fit) background histograms. The shaded band shows the prediction's total uncertainty. The crossed-through points in (b) correspond to the 50 events that are beyond the m_{4l} mass window of 120 GeV < m_{4l} < 130 GeV. The events outside the green signal zone are those that do not meet the m_{34} /m_{12} > 0.85 criterion and include one event that falls within the m_{4l} mass window, [41].*

Table 3: *Expected SM background process event yields and data for the LM H → XX → 4μ (1 GeV < m_X < 15 GeV) selection. The systematic uncertainty in background estimates is highly correlated across different background sources, [41].*

Process	Yield (±stat. ± syst.)
$H \to ZZ^* \to 4\mu$	0.41 ± 0.01 ± 0.03
$ZZ^* \to 4\mu$	0.22 ± 0.04 ± 0.04
VVV/VBS	Negligible
Heavy flavour	0.26 ± 0.09 ± 0.10
Total	0.89 ± 0.10 ± 0.11
Data	0

3.3 ZX analysis: H⟶XX⟶4l (15 GeV < m_X < 55 GeV)

The *ZX* analysis looks for decays of a SM Higgs boson into a *Z* boson and a new boson *X*, where both bosons decay in turn to pairs of electrons or muons. It entails finding two same-flavour opposite-sign lepton pairs with an overall invariant mass consistent with SM Higgs boson decay. The analysis then looks for a peak in the invariant mass distribution of the other pair, which must be roughly consistent with the decay of a *Z* boson.

Figure 4 depicts the final m_{34} distribution for this study, while Table 4 contains the final yields and uncertainties. The modelling of the electron identification efficiency is the source of most of the systematic uncertainty in final states including electrons. The modelling of muon isolation is the source of the most systematic uncertainty in the 4μ channel. With an expected background of 319.7 ± 17.0, a total of 356 events are observed. The test statistic is the profile-likelihood ratio. The $H \to ZZ^*$ background's normalization is allowed to float (as unconstrained nuisance parameter), resulting in a normalization of 1.2 ± 0.16. At roughly m_X = 39 GeV, the highest excess, with a local significance of around 2σ, is found.

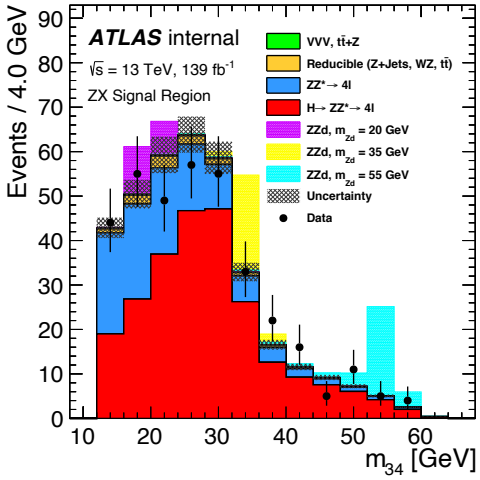

Figure 4: *After the H → ZX⟶ 4l selection, the distribution of m_{34} for data and background events in the mass range 115 GeV < m_{4l} < 130 GeV. The fit provides the background normalization. The shaded band represents the background prediction's overall uncertainty. For certain masses, the signal's expectations are also shown. The signal histograms are layered on top of the background histograms, and the predicted yields are normalized using σ (pp → H → ZZ_d → 4l) = $^{1/10}$ σ_{SM} (pp → H → ZZ* → 4l) = 0.69 fb (ggF process only). For the H⟶ ZZ_d → 4l model, three signal points are shown. The uncertainties of the plotted data are asymmetric and are calculated using Eqs. (40.76) from 2020 Review of Particle Properties [70], [41].*

Table 4: *After the $H \rightarrow ZX \rightarrow 4l$ event selection defined by the mass range 115 GeV < m_{4l} < 130 GeV, the expected and observed numbers of events in each channel. Prior to the fit, the background normalization is performed. The systematic uncertainty in background estimates is highly correlated across different background sources, [41].*

Process	Yield (±stat. ± syst.)		
	$2\ell 2\mu$	$2\ell 2e$	Total
$H \rightarrow ZZ^* \rightarrow 4\ell$	127.9 ± 0.1 ± 3.6	76 ± 0.1 ± 10	204 ± 0.2 ± 12
$ZZ^* \rightarrow 4\ell$	70.2 ± 0.2 ± 1.9	33.0 ± 0.2 ± 3.6	103.3 ± 0.3 ± 4.6
Reducible	4.9 ± 0.1 ± 0.3	5.8 ± 0.3 ± 0.6	10.7 ± 0.3 ± 1.0
$VVV, t\bar{t} + Z$	1.1 ± 0.1 ± 0.04	0.7 ± 0.1 ± 0.1	1.8 ± 0.1 ± 0.1
Total	204.1 ± 0.3 ± 5.5	116 ± 0.5 ± 14	320 ± 0.5 ± 17
Data	237	119	356

4. Limits and Interpretations

For any of the analyses considered, no significant excess is seen above SM background predictions. As a result, the results are interpreted in terms of exclusion limits. First, model-independent limits on fiducial cross sections are set. The benchmark models are then used to determine model-dependent exclusion limits.

Evaluating the limits in the HM and LM $H \rightarrow XX \rightarrow 4l$ analyses necessitates parameterizing the signal distribution as a function of both $\langle m_{ll} \rangle$ and m_X, whereas the $H \rightarrow ZX \rightarrow 4l$ analysis necessitates parameterization as a function of m_{34} and m_X. The signal templates are interpolated between m_X values since simulated events are only generated at discrete values of m_X. This is done using moment morphing [84] for the HM and ZX analyses. The normalization is determined by interpolation of the simulated signal yields, and the distributions at the generated values of m_X are used as templates. Gaussian distributions are fitted to the $\langle m_{ll} \rangle$ distributions at each generated m_X for the LM analysis, and the fit parameters are interpolated in m_X.

A likelihood function consisting of a Poisson factor for each histogram bin, summed over each channel, as well as a Gaussian constraint for each nuisance parameter [85] is used to statistically represent the data:

$$\mathcal{L}(N, \alpha) = \prod_i \text{Pois}\left(\sum_j N_{ij}; \sum_j \mu S_{ij}(\alpha) + B_{ij}(\alpha)\right) \prod_k \text{Gaus}(\alpha_k; s_k, \sigma_k),$$

where N_{ij} is the number of observed events observed in bin i for channel j, α is the set of nuisance parameters, $S_{ij}(\alpha)$ and $B_{ij}(\alpha)$ are the predicted numbers of signal and background events for each bin and channel, μ is the signal strength, and s_k and σ_k are mean and width of the Gaussian constraint for nuisance parameter α_k. Systematic uncertainties are modelled using nuisance parameters that are profiled in the test statistic calculation; systematic uncertainties have a minor impact on the limits.

4.1 Fiducial and Total Cross Section Limits

For the HM, LM, and ZX studies, model-independent cross section limits are calculated using fiducial areas defined on generator-level parameters. These fiducial selections are meant to resemble the signal region selection criteria.

Figure 5 (a) shows the efficiency inside the fiducial regions for the HM and LM analyses using the benchmark $H \rightarrow Z_d Z_d$ model, while the efficiencies for $H \rightarrow aa \rightarrow 4\mu$ over the range 1 GeV < m_a < 15GeV are identical to $H \rightarrow Z_d Z_d \rightarrow 4\mu$ to within a relative difference of 3%. Using the CLs frequentist formalism [86] and the profile likelihood ratio test statistic [87], these efficiencies are used to derive 95% CL upper bounds on the cross section within the fiducial region. Figure 6 depicts the resulting limits. These constraints should hold for any model of the SM Higgs boson decaying to four leptons via two narrow, on-shell intermediate bosons that decay promptly. The model-dependent acceptances for the HM and LM analyses for the $H \rightarrow Z_d Z_d$ and $H \rightarrow aa \rightarrow 4\mu$ models are displayed in Fig. 5 (b). In the HM analysis, the upper limit on the product of the total cross section and decay branching ratio for the benchmark model $\sigma(gg \rightarrow H \rightarrow Z_d Z_d \rightarrow 4l)$ is shown in Fig. 7, whereas in the LM analysis, upper limits on $\sigma(gg \rightarrow H \rightarrow Z_d Z_d \rightarrow 4\mu)$ and $\sigma(gg \rightarrow H \rightarrow aa \rightarrow 4\mu)$ are presented in Fig. 8. These findings are unaffected by assumptions about the Z_d and a bosons' decay branching ratios. Figure 8 (b) is particularly applicable to the scalar case $\sigma(gg \rightarrow H \rightarrow ss \rightarrow 4\mu)$.

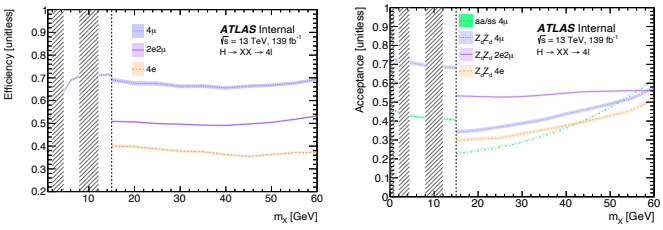

Figure 5: *(a) Model-independent per-channel efficiencies ϵ_c estimated in fiducial volumes in the 1 GeV < m_X < 15 GeV and 15 GeV < m_X < 60 GeV (phase spaces above and below 15 GeV are defined separately). (b) For the $H \rightarrow Z_d Z_d \rightarrow 4l$ and $H \rightarrow aa \rightarrow 4\mu$ processes, model-dependent per-channel fiducial area acceptances. The quarkonia veto regions are shaded areas, [41].*

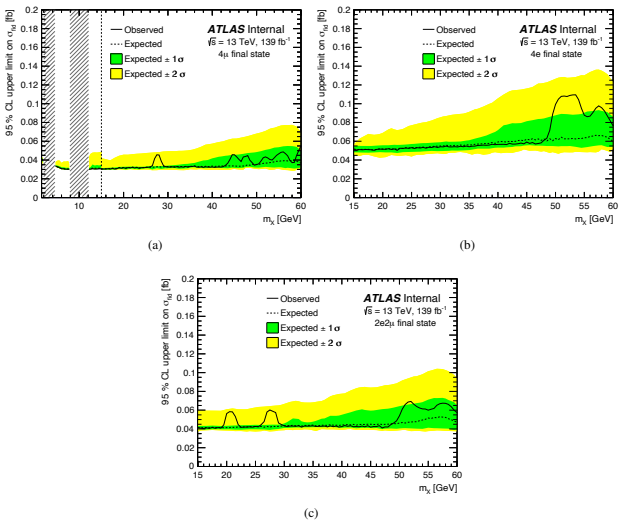

Figure 6: *Per-channel upper limits on fiducial cross sections for the $H \rightarrow XX \rightarrow 4l$ process at 95% CL for the (a) 4μ, (b) 4e, and (c) 2e2μ final states. The change in efficiency produced by the change in fiducial phase-space definition causes the step change in the 4μ channel at m_X = 15 GeV. The quarkonia veto regions are shaded areas, [41].*

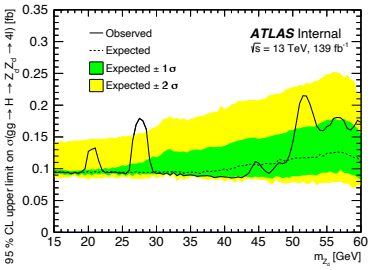

Figure 7: *Upper limits observed and expected for the cross section of the $H \rightarrow Z_dZ_d \rightarrow 4l$ process at 95% CL, assuming SM Higgs boson production via the gluon-gluon fusion process. All final states are combined. HAHM parameters were set to $\kappa=\varepsilon=10^{-4}$ [41].*

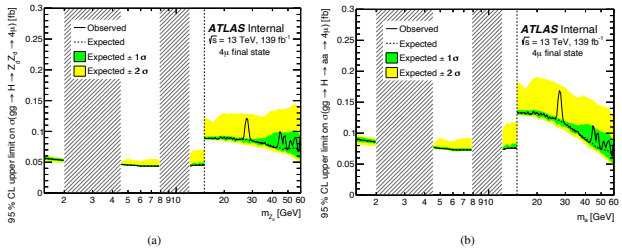

Figure 8: *Upper limits observed and expected for the cross sections of the (a) $H \rightarrow Z_dZ_d \rightarrow 4\mu$ and (b) $H \rightarrow aa \rightarrow 4\mu$ processes at 95% CL, assuming SM Higgs boson generation via the gluon-gluon fusion process. The quarkonia veto regions are the shaded zones. HAHM parameters were set to $\kappa=\varepsilon=10^{-4}$. At m_{Z_d} = 15 GeV, the step shifts are attributable to a transition from the LM to the HM analysis, [41].*

The normalization of the non-resonant $ZZ^* \rightarrow 4l$ background is checked using control samples for limits involving ZX processes, but the normalization of the remaining significant background, $H \rightarrow ZZ^* \rightarrow 4l$, is left to float as an unconstrained nuisance parameter in the limit determination. Figure 9 (a) depicts the model-independent efficiency within the fiducial region, while Figure 10 depicts the 95% CL upper limit on the fiducial region cross section. Figure 9 (b) shows the fiducial region acceptance for the $H \rightarrow ZZ_d \rightarrow 4l$ process, while Figure 11 shows the upper limits on the product of the total cross section and decay branching ratio for the benchmark models $\sigma\,(gg \rightarrow H \rightarrow ZZ_d \rightarrow 4l)$ and $\sigma\,(gg \rightarrow H \rightarrow Za \rightarrow 2l2\mu)$.

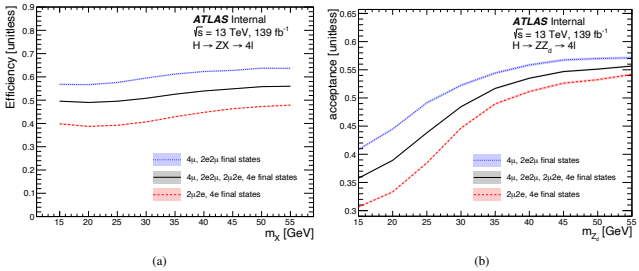

Figure 9: *(a) Model-independent efficiencies ϵ_c for the $H \rightarrow ZX$ process calculated in the fiducial volumes for various combinations of the final state. (b) For different combinations of the final state, model-dependent per-channel fiducial region acceptances for the $H \rightarrow ZZ_d \rightarrow 4l$ process, [41].*

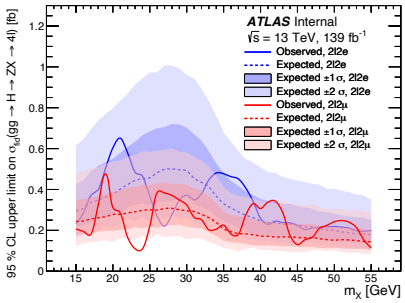

Figure 10: *Per-channel upper limit on the fiducial cross section for the $H \rightarrow ZX \rightarrow 4l$ process at 95% CL, [41].*

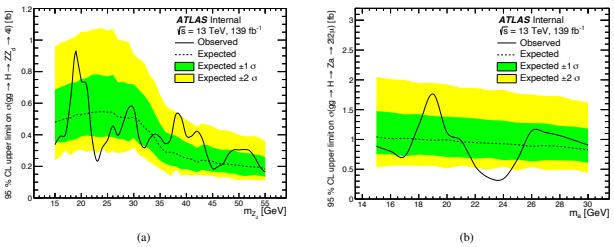

Figure 11: *Upper limits observed and expected for the cross sections of the (a) $H \rightarrow ZZ_d \rightarrow 4l$ and (b) $H \rightarrow Za \rightarrow 2l2\mu$ processes at 95% CL, assuming SM Higgs boson production via the gluon-gluon fusion process. All final states are combined. HAHM parameters were set to $\varepsilon=10^{-4}$ and $\kappa=10^{-10}$[41].*

4.2 Analysis Results – Branching Ratio Limits

The following relations can be used to convert a (model-dependent) cross section limit to a branching ratio limit:

$$\mathrm{BR}(H \to XX \to 4\ell) = \frac{\sigma_{H\to XX\to 4\ell}}{\sigma_H}, \quad (1)$$

$$\mathrm{BR}(H \to XX) = \frac{\mathrm{BR}(H \to XX \to 4\ell)}{\sum_{\ell_1=e,\mu}\sum_{\ell_2=e,\mu}[\mathrm{BR}(X \to 2\ell_1)\mathrm{BR}(X \to 2\ell_2)]}, \quad (2)$$

where $\sigma_{H\to XX\to 4l}$ is the model-dependent total cross section, σ_H is the SM Higgs boson production cross section for the ggF process (48.58 pb for m_H = 125 GeV [88]), and BR($X \to 2l$) is the model-dependent branching ratio for each decay to one lepton flavour. The branching ratios for $Z_d \to ll$ and $a \to \mu\mu$ are taken from the benchmark models [19, 20], where the branching ratios for the two lepton flavors are assumed to be equal for the $Z_d \to ll$ case. Over the range of m_a studied here, the branching ratio for the $a \to \mu\mu$ case varies significantly in a model-dependent way. Figure 12 depicts the resulting branching ratio limits.

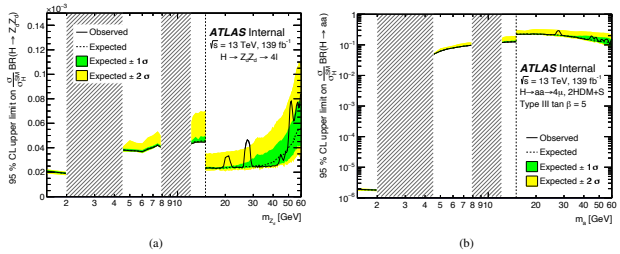

Figure 12: *For (a) the H→ Z_dZ_d process for the benchmark HAHM with κ=ε=10^{-4} and (b) the H → aa process for the benchmark 2HDM+S model, 95% CL upper bounds on the cross section times the model-dependent branching ratio divided by the SM Higgs boson production cross section. The quarkonia veto regions are the shaded zones. At m_{Z_d} = 15 GeV, the step shifts are attributable to a change from the LM to the HM analysis, [41].*

4.3 Analysis Results – Mixing Parameter Limits

The branching ratio limit can also be interpreted as a limit on the effective Higgs mixing parameter κ′, which is defined as (3),

$$\kappa' = \kappa \frac{m_H^2}{|m_H^2 - m_S^2|}, \quad (3)$$

where κ is the Higgs portal coupling and m_S is the mass of the dark Higgs boson. The dependencies on κ and m_S are combined into a single parameter using κ′ instead of κ.

Then, according to Eq. (2.33) of Ref. [19] and assuming $m_S > m_H/2$:

$$\kappa'^2 = \frac{\Gamma_{\mathrm{SM}}}{f(m_{Z_d})} \frac{\mathrm{BR}(H \to Z_dZ_d)}{1 - \mathrm{BR}(H \to Z_dZ_d)}, \quad (4)$$

where Γ_{SM} is the SM width of the 125 GeV Higgs boson,

$$f(m_{Z_d}) = \frac{v^2}{32\pi m_H}\sqrt{1 - \frac{4m_{Z_d}^2}{m_H^2}}\frac{\left(m_H^2 + 2m_{Z_d}^2\right)^2 - 8\left(m_H^2 - m_{Z_d}^2\right)m_{Z_d}^2}{m_H^4}, \quad (5)$$

and $v \approx 246$ GeV is the vacuum expectation value of the Higgs field.

Figure 13 depicts the resulting limit.

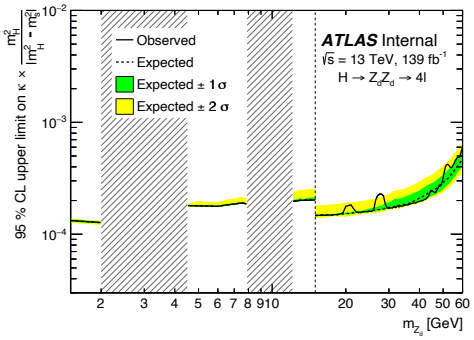

Figure 13: *The upper limit at 95% CL on the effective Higgs mixing parameter $\kappa' = \kappa m_H^2/|m_H^2 - m_S^2|$, with ε set to 10^{-4}. The change in selection from the LM to the HM analysis causes the step change at m_{Z_d} = 15 GeV. The quarkonia veto regions are shaded areas, [41].*

As discussed in Refs. [19, 41], the $H \to ZZ_d$ analysis can also be utilized to determine limits on the Z_d mixing parameter ϵ and the Z - Z_d mass mixing parameter δ. Assuming the SM Higgs boson production cross section, they are given in Fig. 14.

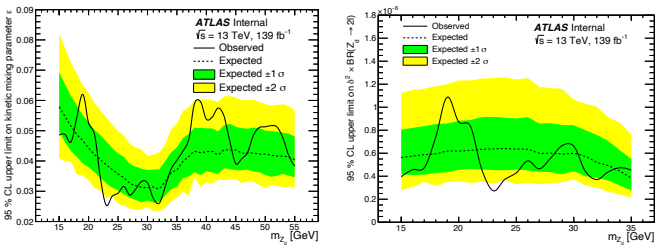

Figure 14: *Using the SM Higgs boson production cross section, the upper limit at 95% CL on (a) the Z_d mixing parameter ε, with κ set to 10^{-10} and (b) the Z-Z_d mass mixing parameter $\delta^2 \times BR$ ($Z_d \rightarrow ll$), [41].*

5. Conclusions

An ATLAS search for exotic decays of the SM Higgs boson into two new spin-1 particles $H \rightarrow Z_d Z_d$, two new spin-0 particles $H \rightarrow aa$, or to a Z boson along with a single Z_d or a was conducted [41]. During the complete Run-2 period of 2015–2018, the ATLAS experiment recorded 139 fb^{-1} of proton-proton collision data at √s = 13 TeV. The first search is for the process $H \rightarrow XX \rightarrow 4l$, where X is either Z_d or a and the energy range is 15 GeV < m_X < 60 GeV. The second search is for the $H \rightarrow XX \rightarrow 4\mu$ process, where 1 GeV < m_X < 15 GeV. The process $H \rightarrow ZX \rightarrow 4l$, where 15 GeV < m_X < 55 GeV, is the subject of the third search. Limits on fiducial and total cross sections are determined after the data is verified to be compatible with the predicted backgrounds in the three searches described. Under the assumptions of gluon-gluon fusion SM Higgs production and prompt decay of the Z_d/a bosons, upper limits on the branching ratio of the Higgs boson to $Z_d Z_d$ and aa as a function of intermediate boson mass are set. Furthermore, constraints are given on the mixing parameters κ', ε, and δ, assuming the HAHM is introduced at the Higgs portal level with very weak kinetic mixing. Due to enhanced statistics, improved lepton reconstruction and identification, and more optimized event selection, the limits provided in this study outperform those in the prior article [42] by a factor of 2–4. This work gives constraints on total cross sections and dark Higgs boson mixing parameters in addition to the results from the previous paper.

References

[1] ATLAS Collaboration, *Observation of a new particle in the search for the Standard Model Higgs boson with the ATLAS detector at the LHC*, Phys. Lett. B **716** (2012) 1, arXiv: 1207.7214 [hep-ex].

[2] CMS Collaboration, *Observation of a new boson at a mass of 125 GeV with the CMS experiment at the LHC*, Phys. Lett. B **716** (2012) 30, arXiv: 1207.7235 [hep-ex].

[3] ATLAS Collaboration, *Measurements of the Higgs boson production and decay rates and constraints on its couplings coupling strengths using p p collision data at √s = 7 and 8 TeV*, Eur. Phys. J. C **76** (2016) 6, arXiv: 1507.04548 [hep-ex].

[4] CMS Collaboration, *Precise determination of the mass of the Higgs boson and tests of compatibility of its couplings with the standard model predictions using proton collisions at 7 and 8 TeV*, Eur. Phys. J. C **75** (2015) 212, arXiv: 1412.8662 [hep-ex].

[5] ATLAS and CMS Collaborations, *Measurements of the Higgs boson production and decay rates and constraints on its couplings from a combined ATLAS and CMS analysis of the LHC p p collision data at √s= 7 and 8 TeV*, JHEP **08** (2016) 045, arXiv: 1606.02266 [hep-ex].

[6] R. E. Shrock and M. Suzuki, *Invisible Decays of Higgs Bosons*, Phys. Lett. B **110** (1982) 250.

[7] M. J. Strassler and K. M. Zurek, *Echoes of a hidden valley at hadron colliders*, Phys. Lett. B **651** (2007) 374, arXiv: hep-ph/0604261.

[8] R. M. Schabinger and J. D. Wells, *Minimal spontaneously broken hidden sector and its impact on Higgs boson physics at the CERN Large Hadron Collider*, Phys. Rev. D **72** (2005) 093007, arXiv: hep-ph/0509209.

[9] B. Patt and F. Wilczek, *Higgs-field portal into hidden sectors*, (2006), arXiv: hep-ph/0605188.

[10] S. Profumo, M. J. Ramsey-Musolf and G. Shaughnessy, *Singlet Higgs phenomenology and the electroweak phase transition*, JHEP **08** (2007) 010, arXiv: 0705.2425 [hep-ph].

[11] N. Blinov, J. Kozaczuk, D. E. Morrissey and C. Tamarit, *Electroweak Baryogenesis from Exotic Electroweak Symmetry Breaking*, Phys. Rev. D **92** (2015) 035012, arXiv: 1504.05195 [hep-ph].

[12] G. Burdman, Z. Chacko, H.-S. Goh and R. Harnik, *Folded supersymmetry and the LEP paradox*, JHEP **02** (2007) 009, arXiv: hep-ph/0609152.

[13] N. Craig, A. Katz, M. Strassler and R. Sundrum, *Naturalness in the Dark at the LHC*, JHEP **07** (2015) 105, arXiv: 1501.05310 [hep-ph].

[14] D. Curtin and C. B. Verhaaren, *Discovering Uncolored Naturalness in Exotic Higgs Decays*, JHEP **12** (2015) 072, arXiv: 1506.06141 [hep-ph].

[15] P. Fayet, *Light spin-1/2 or spin-0 dark matter particles*, Phys. Rev. D **70** (2004) 023514, arXiv: hep-ph/0403226 [hep-ph].

[16] [16] D. P. Finkbeiner and N. Weiner, *Exciting dark matter and the INTEGRAL/SPI 511 keV signal*, Phys. Rev. D **76** (2007) 083519, arXiv: astro-ph/0702587 [astro-ph].

[17] N. Arkani-Hamed, D. P. Finkbeiner, T. R. Slatyer and N. Weiner, *A theory of dark matter*, Phys. Rev. D **79** (2009) 015014, arXiv: 0810.0713 [hep-ph].

[18] E. Dudas, Y. Mambrini, S. Pokorski and A. Romagnoni, *Extra U(1) as natural source of a monochromatic gamma ray line*, JHEP **10** (2012) 123, arXiv: 1205.1520 [hep-ph].

[19] D. Curtin, R. Essig, S. Gori and J. Shelton, *Illuminating dark photons with high-energy colliders*, JHEP **02** (2015) 157, arXiv: 1412.0018 [hep-ph].

[20] D. Curtin, R. Essig, S. Gori, P. Jaiswal, A. Katz et al., *Exotic decays of the 125 GeV Higgs boson*, Phys. Rev. D **90** (2014) 075004, arXiv: 1312.4992 [hep-ph].

[21] H. Davoudiasl, H.-S. Lee, I. Lewis and W. J. Marciano, *Higgs decays as a window into the dark sector*, Phys. Rev. D **88** (2013) 015022, arXiv: 1304.4935 [hep-ph].

[22] H. Davoudiasl, H.-S. Lee and W. J. Marciano, *"Dark" Z implications for parity violation, rare meson decays, and Higgs physics*, Phys. Rev. D **85** (2012) 115019, arXiv: 1203.2947 [hep-ph].

[23] J. D. Wells, *How to Find a Hidden World at the Large Hadron Collider*, (2008), arXiv: 0803.1243 [hep-ph].

[24] S. Gopalakrishna, S. Jung and J. D. Wells, *Higgs boson decays to four fermions through an abelian hidden sector*, Phys. Rev. D **78** (2008) 055002, arXiv: 0801.3456 [hep-ph].

[25] J. A. Evans, S. Gori and J. Shelton, *Looking for the WIMP Next Door*, JHEP **02** (2018) 100, arXiv: 1712.03974 [hep-ph].

[26] V. Silveira and A. Zee, *Scalar Phantoms*, Phys. Lett. B **161** (1985) 136.

[27] M. Pospelov, A. Ritz and M. B. Voloshin, *Secluded WIMP Dark Matter*, Phys. Lett. B **662** (2008) 53, arXiv: 0711.4866 [hep-ph].

[28] P. Draper, T. Liu, C. E. M. Wagner, L.-T. Wang and H. Zhang, *Dark Light-Higgs Bosons*, Phys. Rev. Lett. **106** (2011) 121805, arXiv: 1009.3963 [hep-ph].

[29] S. Ipek, D. McKeen and A. E. Nelson, *Renormalizable model for the Galactic Center gamma-ray excess from dark matter annihilation*, Phys. Rev. D **90** (2014) 055021, arXiv: 1404.3716 [hep-ph].

[30] A. Martin, J. Shelton and J. Unwin, *Fitting the Galactic Center Gamma-Ray Excess with Cascade Annihilations*, Phys. Rev. D **90** (2014) 103513, arXiv: 1405.0272 [hep-ph].

[31] D. Clowe et al., *A direct empirical proof of the existence of dark matter*, Astrophys. J. **648** (2006) L109, arXiv: astro-ph/0608407 [astro-ph].

[32] [32] PAMELA Collaboration, *An anomalous positron abundance in cosmic rays with energies 1.5–100 GeV*, Nature **458** (2009) 607, arXiv: 0810.4995 [astro-ph].

[33] J. Chang et al., An excess of cosmic ray electrons at energies of 300-800 GeV, Nature **456** (2008) 362.

[34] AMS Collaboration, High Statistics Measurement of the Positron Fraction in Primary Cosmic Rays of 0.5–500 GeV with the Alpha Magnetic Spectrometer on the International Space Station, Phys. Rev. Lett. **113** (2014) 121101.

[35] B. A. Dobrescu and K. T. Matchev, *Light axion within the next-to-minimal supersymmetric standard model*, JHEP **09** (2000) 031, arXiv: hep-ph/0008192.

[36] U. Ellwanger, J. F. Gunion, C. Hugonie and S. Moretti, *Towards a No-Lose Theorem for NMSSM Higgs Discovery at the LHC*, (2003), arXiv: hep-ph/0305109.

[37] R. Dermíšek and J. F. Gunion, Escaping the Large Fine-Tuning and Little Hierarchy Problems in the Next to Minimal Supersymmetric Model and h → *aa* Decays, Phys. Rev. Lett. **95** (2005) 041801, arXiv: hep-ph/0502105.

[38] S. Chang, R. Dermíšek, J. F. Gunion and N. Weiner, *Nonstandard Higgs Boson Decays*, Ann. Rev. Nucl. Part. Sci. **58** (2008) 75, arXiv: 0801.4554 [hep-ph].

[39] D. E. Morrissey and A. Pierce, Modified Higgs boson phenomenology from gauge or gaugino mediation in the next-to-minimal supersymmetric standard model, Phys. Rev. D **78** (2008) 075029, arXiv: 0807.2259 [hep-ph].

[40] S. Dawson, C. Englert and T. Plehn, *Higgs physics: It ain't over till it is over*, Phys. Rept. **816** (2019) 1, arXiv: 1808.01324 [hep-ph].

[41] ATLAS Collaboration, Search for Higgs bosons decaying into new spin-0 or spin-1 particles in four-lepton final states with the ATLAS detector with 139 fb^{-1} of pp collision data at √s=13TeV, arXiv: 2110.13673 [hep-ex]

[42] ATLAS Collaboration, The ATLAS Experiment at the CERN Large Hadron Collider, JINST **3** (2008) S08003.

[43] ATLAS Collaboration, *Search for new light gauge bosons in Higgs boson decays to four-lepton final states in pp collisions at √s = 8TeV with the ATLAS detector at the LHC*, Phys. Rev. D **92** (2015) 092001, arXiv: 1505.07645 [hep-ex].

[44] ATLAS Collaboration, *Search for Higgs boson decays to beyond-the-Standard-Model light bosons in four lepton events with the ATLAS detector at √s = 13 TeV*, JHEP **06** (2018) 166, arXiv: 1802.03388 [hep-ex].

[45] ATLAS Collaboration, *Search for Higgs boson decays into two new low-mass spin-0 particles in the 4b channel with the ATLAS detector using p p collisions at √s= 13 TeV*, Phys. Rev. D **102** (2020) 112006, arXiv: 2005.12236 [hep-ex].

[46] ATLAS Collaboration, *Search for Higgs boson decays into pairs of light (pseudo) scalar particles in the γγjj final state in pp collisions at √s=13TeV with the ATLAS detector*, Phys. Lett. B **782** (2018) 750, arXiv: 1803.11145 [hep-ex].

[47] ATLAS Collaboration, *Search for the Higgs boson produced in association with a vector boson and decaying into two spin-zero particles in the H → aa → 4b channel in pp collisions at √s = 13 TeV with the ATLAS detector*, JHEP **10** (2018) 031, arXiv: 1806.07355 [hep-ex].

[48] ATLAS Collaboration, *Search for Higgs boson decays into a pair of light bosons in the bbμμ final state in p p collision at √s = 13 TeV with the ATLAS detector*, Phys. Lett. B **790** (2019) 1, arXiv: 1807.00539 [hep-ex].

[49] ATLAS Collaboration, *Search for Higgs bosons decaying to aa in the μμττ final state in pp* collisions at √s = 8 *TeV with the ATLAS experiment*, Phys. Rev. D **92** (2015) 052002, arXiv: 1505.01609 [hep-ex].

[50] CMS Collaboration, *A search for pair production of new light bosons decaying into muons*, Phys. Lett. B **752** (2016) 146, arXiv: 1506.00424 [hep-ex].

[51] CMS Collaboration, *Search for light bosons in decays of the 125 GeV Higgs boson in proton–proton collisions at √s = 8 TeV*, JHEP **10** (2017) 076, arXiv: 1701.02032 [hep-ex].

[52] CMS Collaboration, *Search for a light pseudoscalar Higgs boson in the boosted μμττ final states* in proton-proton collision at √s = *13 TeV*, JHEP **08** (2020) 139, arXiv: 2005.08694 [hep-ex].

[53] ATLAS Collaboration, *Combination of Searches for Invisible Higgs Boson Decays with the ATLAS Experiment*, Phys. Rev. Lett. **122** (2019) 231801, arXiv: 1904.05105 [hep-ex].

[54] CMS Collaboration, *Search for invisible decays of a Higgs boson produced through vector boson* $\sqrt{s} = 13$ *TeV*, Phys. Lett. B **793** (2019) 520, arXiv: 1809.05937 [hep-ex].

[55] P. Galison and A. Manohar, *Two Z's or not two Z's?*, Phys. Lett. B **136** (1984) 279.

[56] B. Holdom, *Two U(1)'s and ϵ charge shifts*, Phys. Lett. B **166** (1986) 196.

[57] K. R. Dienes, C. F. Kolda and J. March-Russell, *Kinetic mixing and the supersymmetric gauge hierarchy*, Nucl. Phys. B **492** (1997) 104, arXiv: hep-ph/9610479 [hep-ph].

[58] ATLAS Collaboration, Search for long-lived neutral particles decaying into lepton jets in *proton–proton collisions at* $\sqrt{s} = 8$ *TeV with the ATLAS detector*, JHEP **11** (2014) 088, arXiv: 1409.0746 [hep-ex].

[59] ATLAS Collaboration, *A search for prompt lepton-jets in p p collisions at* $\sqrt{s} = 8$ *TeV with the ATLAS detector*, JHEP **02** (2016) 062, arXiv: 1511.05542 [hep-ex].

[60] ATLAS Collaboration, *Search for massive, long-lived particles using multitrack displaced vertices or displaced lepton pairs in pp collisions at* $\sqrt{s} = 8$*TeV with the ATLAS detector*, Phys. Rev. D **92** (2015) 072004, arXiv: 1504.05162 [hep-ex].

[61] CMS Collaboration, *Search for long-lived particles that decay into final states containing two electrons or two muons in proton–proton collisions at* $\sqrt{s} = 8$ *TeV*, Phys. Rev. D **91** (2015) 052012, arXiv: 1411.6977 [hep-ex].

[62] ATLAS Collaboration, Search for long-lived particles in final states with displaced dimuon vertices in $p\,p$ collisions at $\sqrt{s} =$ 13 TeV with the ATLAS detector, Phys. Rev. D **99** (2019) 012001, arXiv: 1808.03057 [hep-ex].

[63] ATLAS Collaboration, Search for displaced vertices of oppositely charged leptons from decays of *long-lived particles in p p collisions at* $\sqrt{s} = 13$ *TeV with the ATLAS detector*, Phys. Lett. B **801** (2020) 135114, arXiv: 1907.10037 [hep-ex].

[64] ATLAS Collaboration, Search for light long-lived neutral particles produced in $p\,p$ collisions at $\sqrt{s} = 13$ TeV and decaying into collimated leptons or light hadrons with the ATLAS detector, Eur. Phys. J. C **80** (2020) 450, arXiv: 1909.01246 [hep-ex].

[65] ATLAS Collaboration, Constraints on mediator-based dark matter and scalar dark energy models using $\sqrt{s} = 13$TeV pp collision data collected by the ATLAS detector, JHEP **05** (2019) 142, arXiv: 1903.01400 [hep-ex].

[66] CMS Collaboration, A search for pair production of new light bosons decaying into muons in proton–proton collisions at 13 TeV, Phys. Lett. B **796** (2019) 131, arXiv: 1812.00380 [hep-ex].

[67] A. Belyaev, J. Pivarski, A. Safonov, S. Senkin and A. Tatarinov, *LHC discovery potential of the lightest NMSSM Higgs in the* $h_1 \to a_1 a_1 \to 4\mu$ *channel*, Phys. Rev. D **81** (2010) 075021, arXiv: 1002.1956 [hep-ph].

[68] J.F. Gunion, B. Grazadowski, H.E. Haber, J. Kalinowski, *Limits from LEP Data on CP-Violating Nonminimal Higgs Sectors*, Phys. Rev. Lett. **79** (1997) 982, arXiv: hep-ph/9704410.

[69] G. Belanger, B. Dumont, U. Ellwanger, J. F. Gunion and S. Kraml, *Global fit to Higgs signal strengths and couplings and implications for extended Higgs sectors*, Phys. Rev. D **88** (2013) 075008, arXiv: 1306.2941 [hep-ph].

[70] P. Zyla et al., *Review of Particle Physics*, Prog. Theor. Exp. Phys. **2020** (2020) 083C01.

[71] ATLAS Collaboration, *Measurement of the Higgs boson coupling properties in the* $H \to Z\,Z^* \to 4l$ *decay channel at* $\sqrt{s} = 13$ *TeV with the ATLAS detector*, JHEP **03** (2018) 095, arXiv: 1712.02304 [hep-ex].

[72] ATLAS Collaboration, *Measurement of inclusive and differential cross sections in the* $H \to Z\,Z^* \to 4l$ *decay channel in p p collisions at* $\sqrt{s} = 13$ *TeV with the ATLAS detector*, JHEP **10** (2017) 132, arXiv: 1708.02810 [hep-ex].

[73] ATLAS Collaboration, *Luminosity determination in pp collisions at* $\sqrt{s} = 13$*TeV using the ATLAS detector at the LHC*, ATLAS-CONF-2019-21, 2019, url:https://cds.cern.ch/record/2677054

[74] G. Avoni et al., *The new LUCID-2 detector for luminosity measurement and monitoring in ATLAS*, JINST **13** (2018) P07017.

[75] ATLAS Collaboration, Electron and photon performance measurements with the ATLAS detector using the 2015–2017 LHC proton–proton collision data, JINST **14** (2019) P12006, arXiv: 1908.00005 [hep-ex].

[76] ATLAS Collaboration, *Muon reconstruction and identification efficiency in ATLAS using the full Run 2 p p collision data set at* $\sqrt{s} = 13$ *TeV*, Eur. Phys. J. C **81** (2021) 578, arXiv: 2012.00578 [hep-ex].

[77] S. Dittmaier et al., *Handbook of LHC Higgs Cross Sections: 1. Inclusive Observables*, CERN-2011-002 (2011), arXiv: 1101.0593 [hep-ph].

[78] ATLAS Collaboration, Multi-Boson Simulation for 13 TeV ATLAS Analyses, ATL-PHYS-PUB-2017-005, 2017, url: https://cds.cern.ch/record/2261933.

[79] T. Gleisberg and S. Höche, *Comix, a new matrix element generator*, JHEP **12** (2008) 039, arXiv: 0808.3674 [hep-ph].

[80] S. Schumann and F. Krauss, *A parton shower algorithm based on Catani–Seymour dipole factorisation*, JHEP **03** (2008) 038, arXiv: 0709.1027 [hep-ph].

[81] S. Höche, F. Krauss, M. Schönherr and F. Siegert, *QCD matrix elements + parton showers. The NLO case*, JHEP **04** (2013) 027, arXiv: 1207.5030 [hep-ph].

[82] F. Cascioli, P. Maierhöfer and S. Pozzorini, *Scattering Amplitudes with Open Loops*, Phys. Rev. Lett. **108** (2012) 111601, arXiv: 1111.5206 [hep-ph].

[83] F. Caola, K. Melnikov, R. Röntsch and L. Tancredi, *QCD corrections to ZZ production in gluon fusion at the LHC*, Phys. Rev. D **92** (2015) 094028, arXiv: 1509.06734 [hep-ph].

[84] M. Baak, S. Gadatsch, R. Harrington and W. Verkerke, *Interpolation between multi-dimensional histograms using a new non-linear moment morphing method*, Nucl. Instrum. Meth. A **771** (2015) 39, arXiv: 1410.7388 [physics.data-an].

[85] K. Cranmer, A. Shibata, W. Verkerke, L. Moneta and G. Lewis, *HistFactory: A tool for creating statistical models for use with RooFit and RooStats*, tech. rep., 2012, url: https://cds.cern.ch/record/1456844.

[86] A. L. Read, *Presentation of search results: the CLS technique*, J. Phys. G **28** (2002) 2693.

[87] G. Cowan, K. Cranmer, E. Gross and O. Vitells, *Asymptotic formulae for likelihood-based tests of new physics*, Eur. Phys. J. C **71** (2011) 1554, arXiv: 1007.1727 [physics.data-an], Erratum: Eur. Phys. J. C **73** (2013) 2501.

[88] C. Anastasiou et al., *High precision determination of the gluon fusion Higgs boson cross-section at the LHC*, JHEP **05** (2016) 058, arXiv: 1602.00695 [hep-ph].